Sensitivity Estimates for the SPICA Mid-Infrared Instrument (SMI)

Itsuki Sakon*[a], Hidehiro Kaneda[b], Shinki Oyabu[b], Daisuke Ishihara[b], Takehiko Wada[c], Naofumi Fujishiro[d,e], and SMI consortium

[a]Department of Astronomy, Graduate School of Science, University of Tokyo, 7-3-1 Hongo, Bunkyo-ku, Tokyo 113-0033, Japan
[b]Department of Physics, Nagoya University, Furo-cho, Chikusa-ku, Nagoya, Aichi 464-8602, Japan
[c]Institute of Space and Astronautical Science, Japan Aerospace Exploration Agency, 3-1-1 Yoshinodai, Chuo-ku, Sagamihara, Kanagawa 252-5210, Japan
[d]Deprtment of Physics, Faculty of Science, Kyoto-Sangyo University, Motoyama, Kamigamo, Kita-Ku, Kyoto-City 603-8555, Japan
[e]Kyoto-Nijikoubou, 17-203 Minami Oosagicho, Iwakura, Sakyo-ku, Kyoto 606-0003, Japan

*isakon@astron.s.u-tokyo.ac.jp; phone +81-3-5841-4276 / fax +81-5841-7644

ABSTRACT

We present the latest results of the sensitivity estimate for spectrometers of the SPICA Mid-Infrared Instrument (SMI). SMI has three spectroscopic channels; low resolution spectrometer (LRS), medium resolution spectrometer (MRS) and high resolution spectrometer (HRS). Taking account of the results of optical design of each spectrometer and the latest information of the expected performance of detector arrays, the continuum sensitivity for a point source, the continuum sensitivity for an extended source, the line sensitivity for a point source, the line sensitivity for an extended source, and the saturation limit are calculated for LRS, MRS and HRS and are provided in this paper.

Keywords: SPICA, Spectrometers, Sensitivity

1. INTRODUCTION

SPICA Mid-Infrared Instrument (SMI; Kaneda et al. 2016) has three spectroscopic channels; low resolution spectrometer (LRS), medium resolution spectrometer (MRS) and high resolution spectrometer (HRS). LRS is a multi-slits prism spectrometer covering the wavelength range from 17μm to 37μm with a spectral resolution of R=50—120. The spectra along the four long slits, each of which has a size of 3".7 width by 10' length, are obtained on the Si:Sb detector array. MRS is a crossed Echelle grating spectrometer covering the wavelength range from 18μm to 36μm with R~1000. The spectra over six different orders from m=6th to 11th along a long slit, which has a size of 3".7 width by 60" length, are obtained on the Si:Sb detector array. HRS is a crossed Echelle immersion grating spectrometer covering the wavelength range from 12μm to 18.7μm with R~27,000. The spectra over 34 different orders from 85th to 118th, which successively covers the wavelengths from 12.14μm to 17.03μm, and those over 8 different orders from 77th to 84th, which partly covers the wavelengths from 17.03μm to 18.75μm, are obtained on the Si:As detector array.

2. PARAMETERS AND ASSUMPTIONS

2.1 Telescope Parameters

The effective area of the primary mirror, S_{tel}, is given by $\pi \times (D/2)^2 \times (1-\eta_{secondary})$, where $D=2.5$ m case is assumed in the following calculation and $\eta_{secondary} = 20$ % is a fraction of area masked by the secondary mirror and support structures.

2.2 Exposure Time

The longest exposure time t_{exp} is defined so that the mean number of pixels affected by cosmic ray hit events during an exposure should not exceed $\eta=1/25$ (4%) of the whole pixels of a detector array. The Si:Sb detectors used in LRS and MRS have an array size of 1024 pixels by 1024 pixels with an actual pixel size of 18μm×18μm. The Si:As detector array used in HRS has an array size of 1024 pixels by 1024 pixels with an actual pixel size of 25μm by 25μm. The cosmic-ray hit event rate at L2 point is assumed as $\chi_{CR}=5\times10^4$ m^{-2} sec^{-1} (Swinyard et al. 2004). Assuming that the number of pixels affected by a single cosmic-ray hit event be 4 pixels, the number of pixels affected by the cosmic ray hit events during an exposure time can be given by $4\chi_{CR}A_{det}t_{exp}$, where A_{det} is an area of each detector; $A_{Si:Sb}=(18\times10^{-6}\times1024)^2$ m^{-2} and $A_{Si:As}=(25\times10^{-6}\times1024)^2$ m^{-2}. The Si:Sb detector allow the exposure time shorter than 617.3 sec and the Si:As shorter than 320.0 sec. In the following calculations, therefore, the longest exposure time t_{exp} is set to $t_{exp} = 600$ sec for the Si:Sb detectors and to $t_{exp} = 300$ sec for the Si:As detector at default. The shortest ramp duration t_{exp}^{short} is set to $t_{exp}^{short}=2$ sec for both the Si:As and Si:Sb detectors.

2.3 Detector Performance

The expected values of detector dark current i^{dark}_{det} for 1K×1K Si:Sb BIB detector and 1K×1K Si:As BIB detector are assumed as $i^{dark}_{Si:Sb}=0.8$ e^- sec^{-1} $pixel^{-1}$ and $i^{dark}_{Si:As}=0.06$ e^- sec^{-1} $pixel^{-1}$, respectively. The expected noise in CDS readout for Si:Sb detector and Si:As detector are expected as 100 e^- and 40 e^-, respectively. We note that these CDS readout noise can be reduced down to 1/4 by means of Fowler-16 sampling and, therefore, $n_{Si:Sb}^{read}=25$ e^- and $n_{Si:As}^{read}=10$ e^- are adopted as the readout noise (n_{det}^{read}) expected for Si:Sb detector and Si:As detector in the course of sensitivity estimate. The saturation full well of the detector is assumed as 1.0×10^5 e^- per exposure for Si:Sb and 2.0×10^5 e^- per exposure for Si:As detectors. In both cases, the linearity for the response is assumed to be ensured below $\eta_{linearity}=1.0$ of the full well after executing appropriate correction. The detector quantum efficiency profiles, $\eta_{DQE}(\lambda)$, for Si:Sb detector and Si:As detector used in our calculations are shown in Figure 1.

2.4 Background

We assume that the background emission in the mid-infrared wavelengths is dominated by zodiacal light emission. In the following calculations, the high background case assumes the condition of the ecliptic plane at $\beta=0.0$ deg and $\varepsilon=60$ deg while the low background case assumes the condition of the ecliptic pole at $\beta=90$ deg. The zodiacal emission in the high background case is modeled with blackbody of $T=268.5$ K normalized to 80 MJy/sr at 25μm, while that in the low background case is molded with blackbody of $T=274.0$ K normalized to 15 MJy/sr at 25 μm taking account of the results of observations with ISO and IRTS (i.e., Reach et al. 2003; Ootsubo et al. 2000)

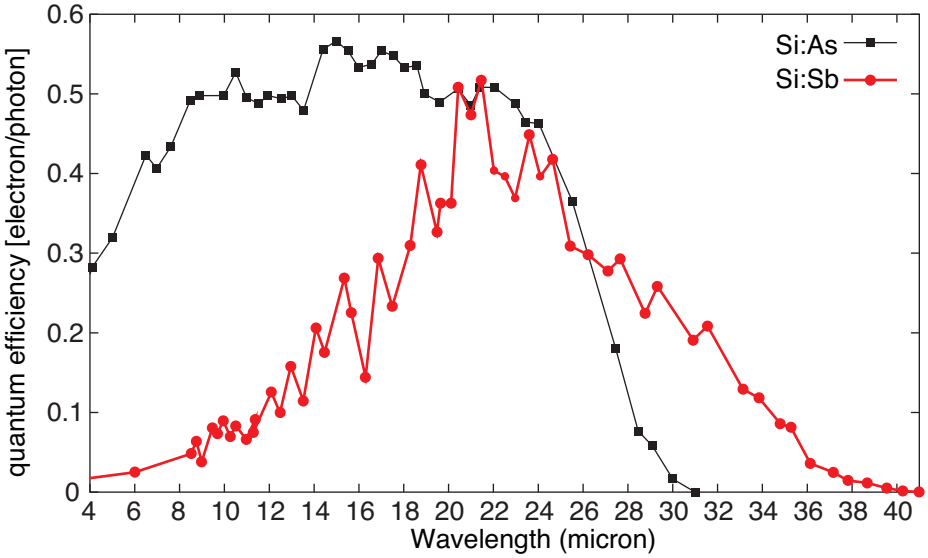

Figure 1. The detector quantum efficiency, $\eta_{DQE}(\lambda)$, for Si:Sb detector and Si:As detector used in our calculations.

3. LOW RESOLUTION SPECTROMETER (LRS)

3.1 Spectral Format

LRS has multi-slit spectroscopic capability using four parallel long slits, each of which has a size of 10' length and 3.7" width. The spectral format on the 1K×1K Si:Sb BIB detector array is given in Figure 2 by showing 20 spectra (#01—#20) collected at 5 different positions on each slit (e.g., the spectra labeled with #09, #10, #11 and #12 are those collected at the center of each slit). The plate scale is 0.7 arcsec pix^{-1}. We note that the point spread function and the pixel-to-wavelength relations (i.e., $\lambda=\Lambda(X)$) are variable both among the different positions along a slit and among the slits. Therefore, in the following sensitivity estimates, we representatively show the results at position #11 for the best quality case and at position #1 for the worst quality case.

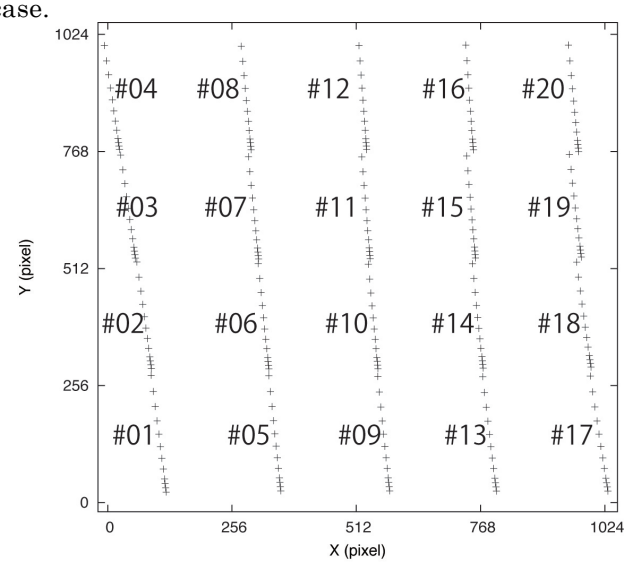

Figure 2. The spectral format of SMI/LRS showing the dispersion directions of the 20 spectra (collected at 5 different positions on each of the four slits) on the 1K×1K Si:Sb BIB detector array.

3.2 Noise Equivalent Electron per Pixel per Exposure

The 1-σ noise equivalent electrons per pixel per second at a certain pixel position X, $\phi^{NE}(X)$ e^{-} sec^{-1}, is calculated by the Poisson noise of electrons which generate per pixel per exposure and the readout noise $n_{Si:Sb}^{read}$. In the case of LRS, $\phi^{NE}(X)$ satisfies the following equation

$\phi^{NE}(X)\ t_{exp} = \{\phi^{NE}(X)\ t_{exp} + \phi^{BG}(X)\ t_{exp} + i_{Si:Sb}^{dark}\ t_{exp} + (n_{Si:Sb}^{read})^2\}^{1/2}$,

where $\phi^{BG}(X)$ is a number of electrons generated at X by uniform background. Taking account of the available information of the point spread function, pixel-to-wavelength relations (i.e., λ=Λ(X)) and the efficiency of the grating based on the latest design of optics, the values of $\phi^{NE}(X)\ t_{exp}$, $\{\phi^{BG}(X)\ t_{exp}\}^{1/2}$, $(i_{Si:Sb}^{dark}\ t_{exp})^{1/2}$ and $n_{Si:Sb}^{read}$ are calculated and shown in Figure 3 as a function of λ(=Λ(X)).

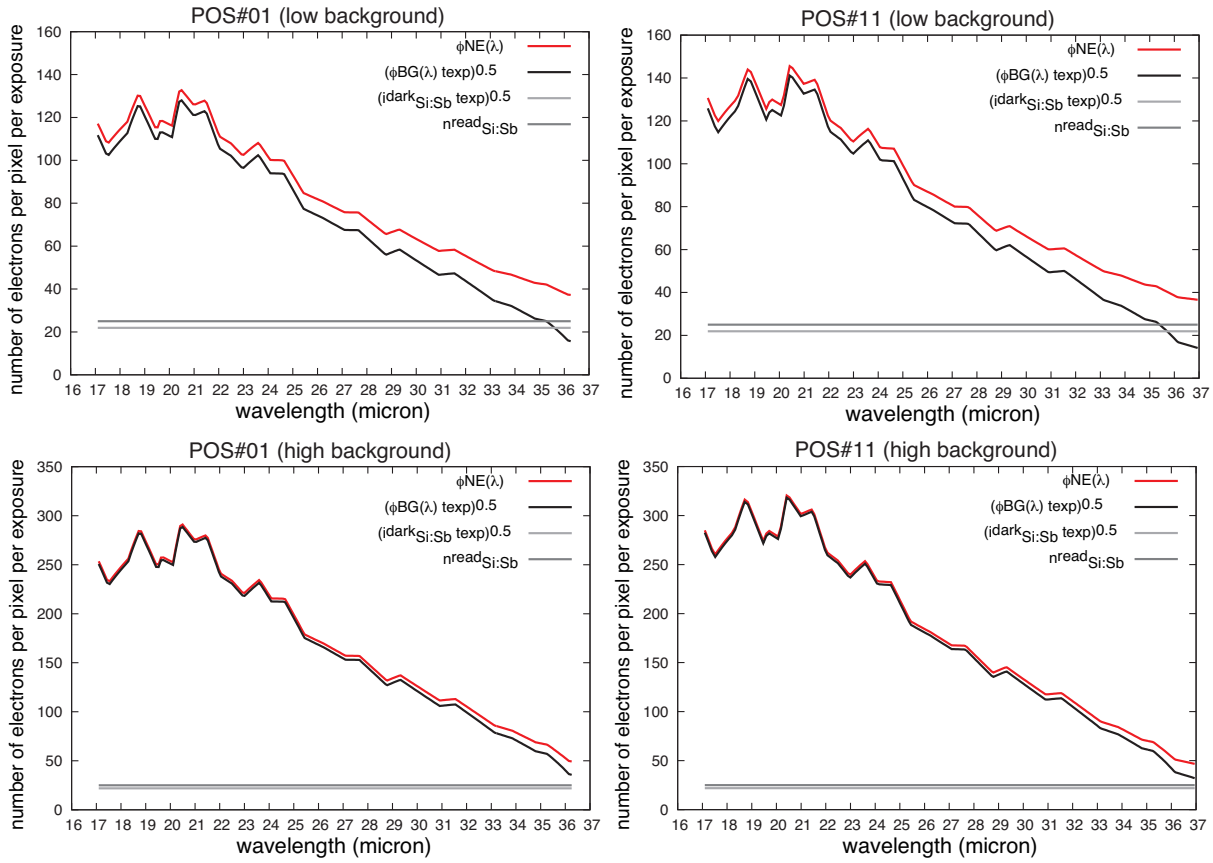

Figure 3. The plots of $\phi^{NE}(X)\ t_{exp}$, $\{\phi^{BG}(X)\ t_{exp}\}^{1/2}$, $(i_{Si:Sb}^{dark}\ t_{exp})^{1/2}$ and $n_{Si:Sb}^{read}$ as a function of $\lambda\ (=\Lambda(X))$.

3.3 Sensitivity Estimate for the SMI/LRS

The 1-hour 5-σ sensitivities of SMI/LRS for a continuum emission of a point source ($s^{PSC}(\lambda)$ in units of μJy) at positions #01 and #11 calculated for the adopted spectral resolution of R=λ/Δλ. the 1-hour 5-σ sensitivities of SMI/LRS for a line emission of a point source ($s^{PSL}(\lambda)$ in units of Wm^{-2}) at positions #01 and #11, the 1-hour 5-σ sensitivities of SMI/LRS for a continuum emission of an extended source ($s^{ESC}(\lambda)$ in units of MJy/sr) at positions #01 and #11 calculated for the adopted spectral resolution of R=λ/Δλ and the 1-hour 5-σ sensitivities of SMI/LRS for a line emission of an extended source ($s^{ESL}(\lambda)$ in units of $Wm^{-2}sr^{-1}$) at positions #01 and #11 are shown in Figures 4, 5, 6 and 7, respectively. The calculations are made independently for both the low- and high-background cases.

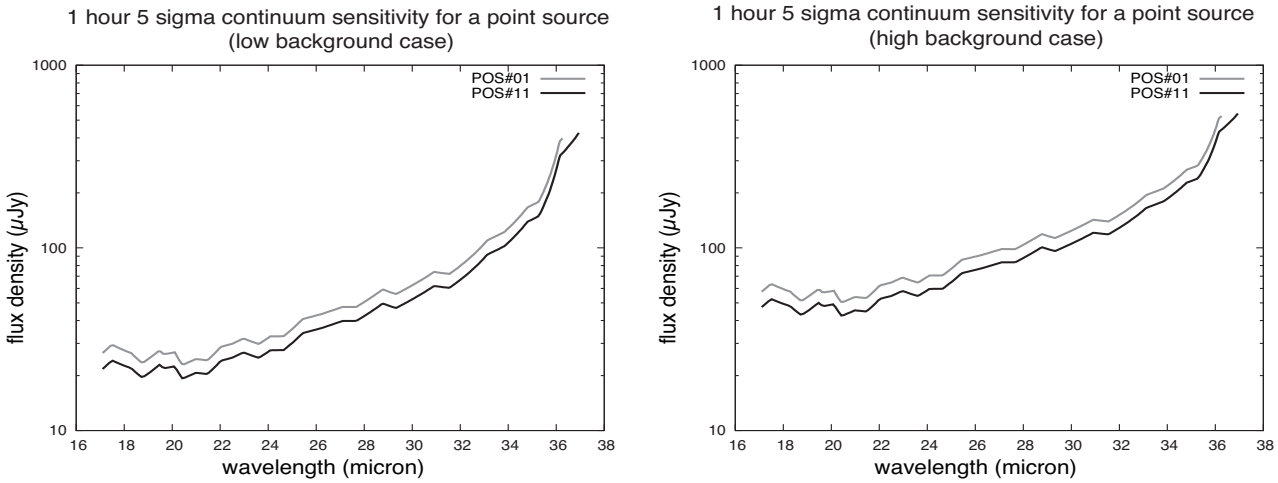

Figure 4. 1-hour 5-σ sensitivities of SMI/LRS for a continuum emission of a point source $s^{PSC}(\lambda)$ in μJy at positions #01 and #11 calculated for the adopted spectral resolution of R=λ/Δλ.

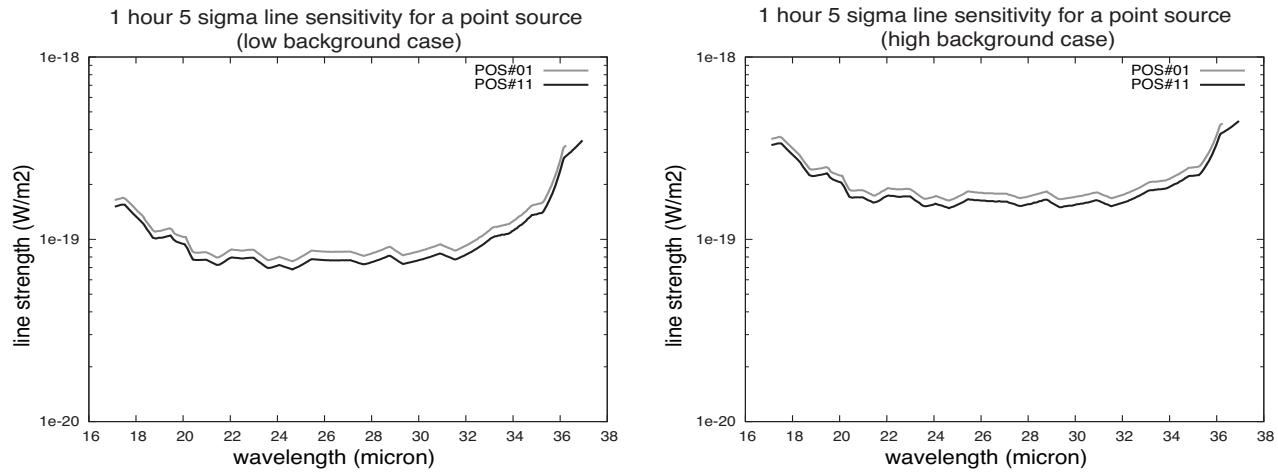

Figure 5. 1-hour 5-σ sensitivities of SMI/LRS for a line emission of a point source $s^{PSL}(\lambda)$ in Wm^{-2} at positions #01 and #11

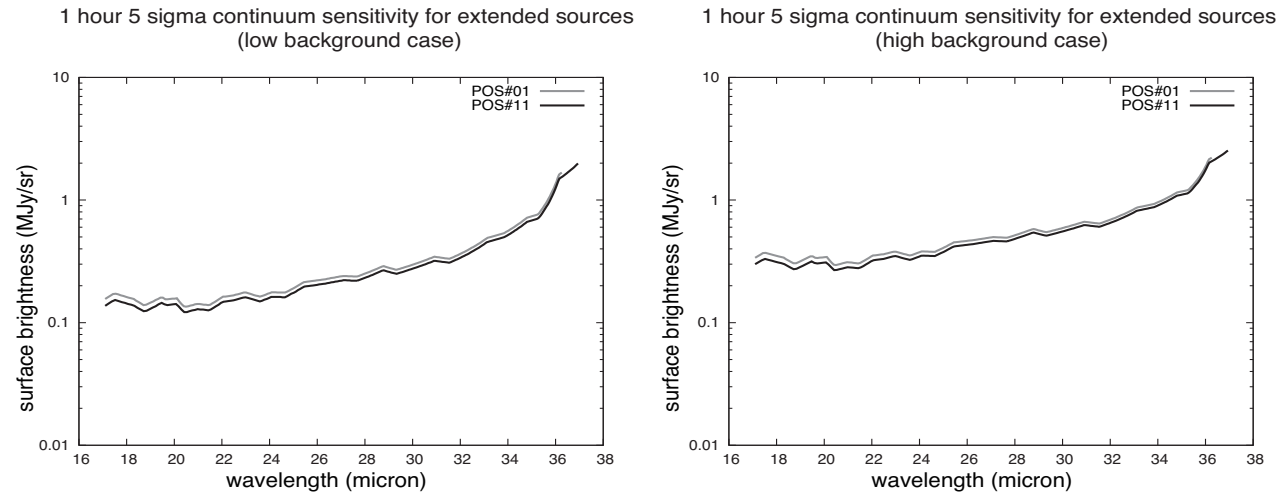

Figure 6. 1-hour 5-σ sensitivities of SMI/LRS for a continuum emission of an extended source $s^{ESC}(\lambda)$ in MJy/sr at positions #01 and #11 calculated for the adopted spectral resolution of R=λ/Δλ.

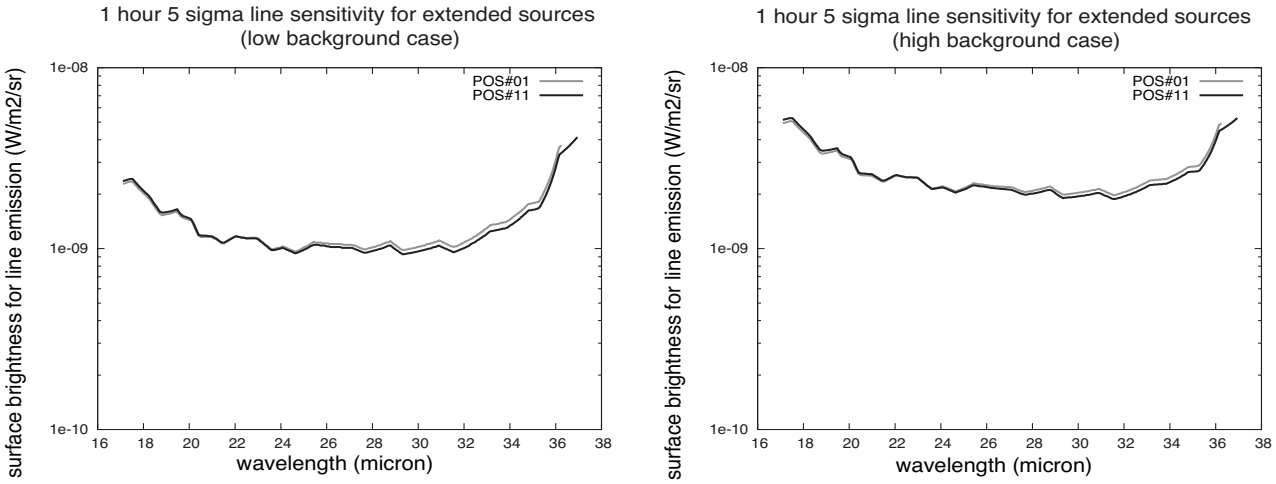

Figure 7. 1-hour 5-σ sensitivities of SMI/LRS for a line emission of an extended source $s^{ESL}(\lambda)$ in Wm^{-2} sr^{-1} at positions #01 and #11

3.4 Saturation limit of SMI/LRS

The saturation limits for a continuum emission of a point source ($S^{PSC}(\lambda)$ in units of Jy) at positions #01 and #11 are shown in Figure 8. The calculations are made independently for both the low- and high-background cases. We note that the datapoints for both cases are indistinguishable at the scale of this plot.

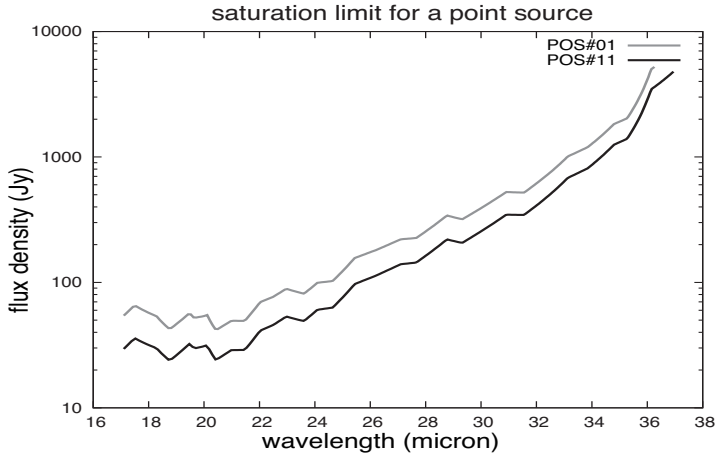

Figure 8. The saturation limit of SMI/LRS for a continuum emission of a point source $S^{PSC}(\lambda)$ in Jy at positions #01 and #11

4. MEDIUM RESOLUTION SPECTROMETER (MRS)

4.1 Spectral Format

MRS has a long slit with a size of 60" length and 3.7" width. The incoming light through the long slit is cross dispersed via the Echelle grating and cross disperser so that the spectrum over six different orders from m=6th to 11th falls on the 1K×1K Si:Sb BIB detector array. The spectral format on the detector array is shown in Figure 9. The plate scale is 0.725 arcsec pix^{-1}.

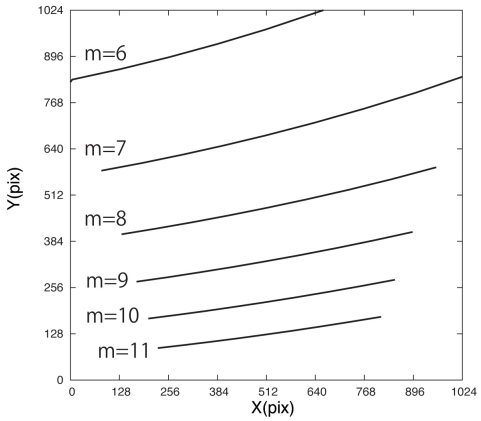

Figure 9. The spectral format of SMI/MRS showing the dispersion directions of the spectrum over six different orders from m=6th to 11th on the 1K×1K Si:Sb BIB detector array.

4.2 Noise Equivalent Electron per Pixel per Exposure

The 1-σ noise equivalent electrons per pixel per second at a certain pixel position X in the m^{th} order spectrum of SMI/MRS, $\phi_m^{NE}(X)$ e^- sec^{-1}, satisfies the following equation

$\phi_m^{NE}(X)\, t_{exp} = \{\phi_m^{NE}(X)\, t_{exp} + \phi_m^{BG}(X)\, t_{exp} + i_{Si:Sb}^{dark}\, t_{exp} + (n_{Si:Sb}^{read})^2\}^{1/2}$,

where $\phi_m^{BG}(X)$ is a number of electrons generated at X in the m^{th} order spectrum of MRS by uniform background. Taking account of the available information of the point spread function, wavelength-to-pixel relations for the m^{th} order spectrum (i.e., $\lambda=\Lambda_m(X)$) and the efficiency of the Echelle grating and cross disperser based on the latest design of optics, the values of $\phi_m^{NE}(X)\, t_{exp}$, $\{\phi_m^{BG}(X)\, t_{exp}\}^{1/2}$, $(i_{Si:Sb}^{dark}\, t_{exp})^{1/2}$ and $n_{Si:Sb}^{read}$ are calculated and shown in Figure 10 as a function of $\lambda\,(=\Lambda_m(X))$.

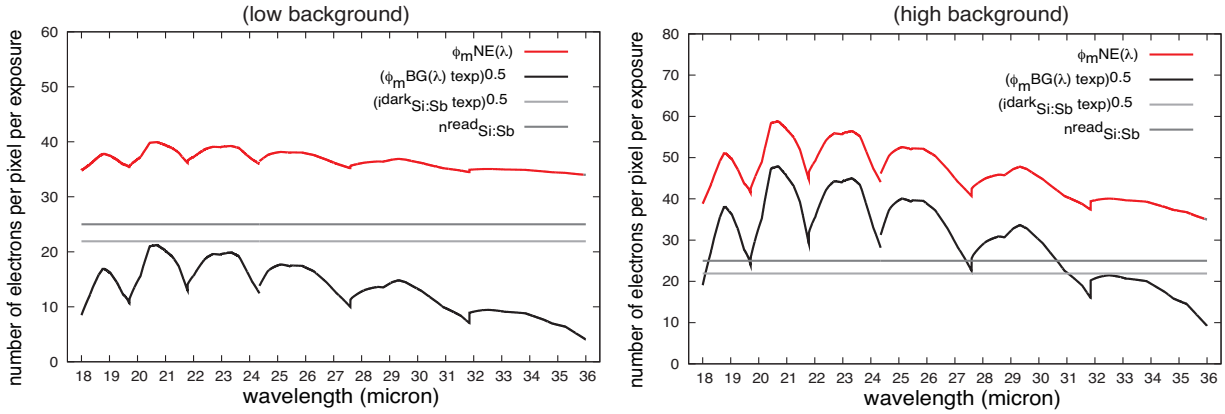

Figure 10. The plots of $\phi_m^{NE}(X)\, t_{exp}$, $\{\phi_m^{BG}(X)\, t_{exp}\}^{1/2}$, $(i_{Si:Sb}^{dark}\, t_{exp})^{1/2}$ and $n_{Si:Sb}^{read}$ as a function of $\lambda\,(=\Lambda_m(X))$..

4.3 Sensitivity Estimate for the SMI/MRS

The 1-hour 5-σ sensitivities of SMI/MRS for a continuum emission of a point source ($s^{PSC}(\lambda)$ in units of μJy) calculated for the adopted spectral resolution of R=λ/Δλ. the 1-hour 5-σ sensitivities of SMI/MRS for a line emission of a point source ($s^{PSL}(\lambda)$ in units of Wm^{-2}), the 1-hour 5-σ sensitivities of SMI/MRS for a continuum emission of an extended source ($s^{ESC}(\lambda)$ in units of MJy/sr) calculated for the adopted spectral resolution of R=λ/Δλ and the 1-hour 5-σ sensitivities of SMI/MRS for a line emission of an extended source ($s^{ESL}(\lambda)$ in units of $Wm^{-2}sr^{-1}$) are shown in Figures 11, 12, 13 and 14, respectively. The calculations are made independently for both the low- and high-background cases.

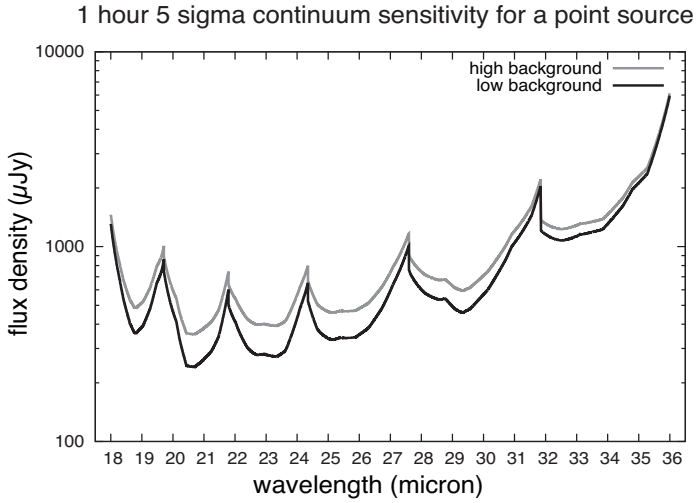

Figure 11. 1-hour 5-σ sensitivities of SMI/MRS for a continuum emission of a point source $s^{PSC}(\lambda)$ in μJy calculated for the adopted spectral resolution of R=λ/Δλ.

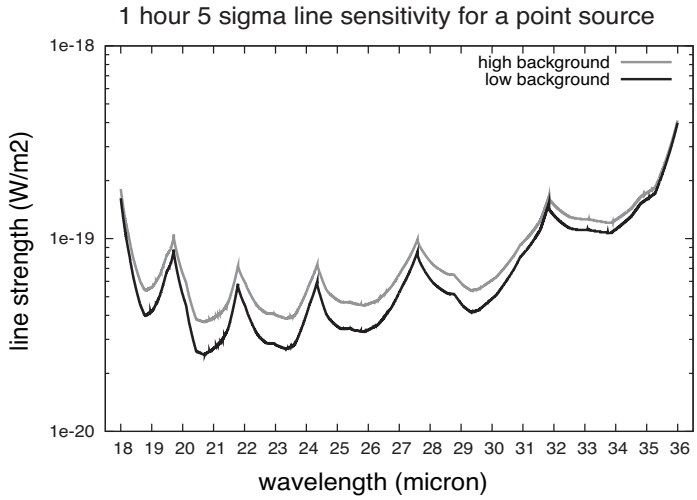

Figure 12. 1-hour 5-σ sensitivities of SMI/MRS for a line emission of a point source $s^{PSL}(\lambda)$ in Wm^{-2}.

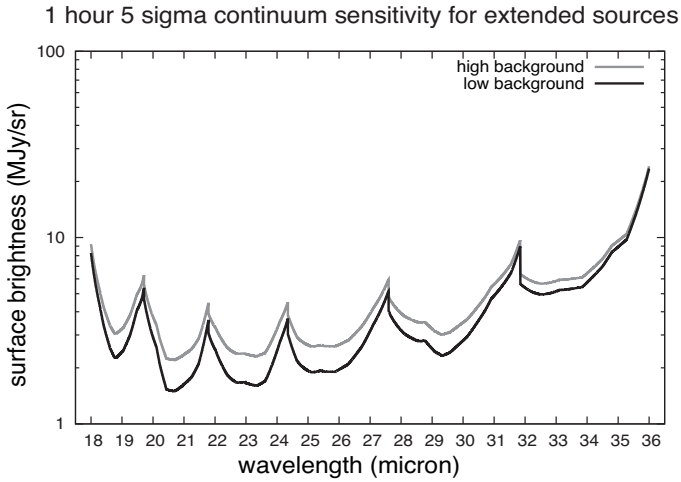

Figure 13. 1-hour 5-σ sensitivities of SMI/MRS for a continuum emission of an extended source $s^{ESC}(\lambda)$ in MJy/sr calculated for the adopted spectral resolution of R=λ/Δλ.

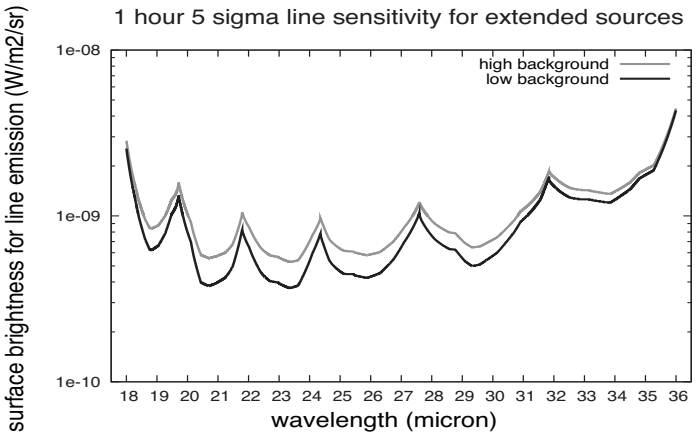

Figure 14. 1-hour 5-σ sensitivities of SMI/MRS for a line emission of an extended source $s^{ESL}(\lambda)$ in Wm^{-2} sr^{-1}.

4.4 Saturation limit of SMI/MRS

The saturation limits of SMI/MRS for a continuum emission of a point source ($S^{PSC}(\lambda)$ in units of Jy) are shown in Figure 15. The calculations are made independently for both the low- and high-background cases. We note that the data points for both cases are indistinguishable at the scale of this plot.

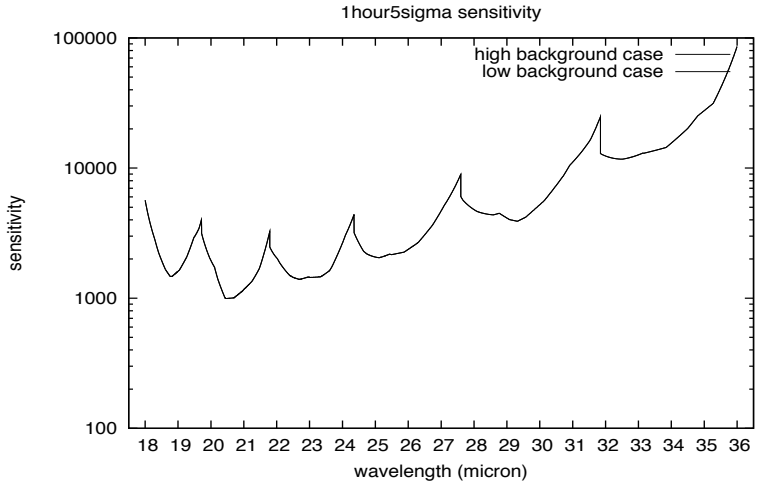

Figure 15. The saturation limit of SMI/MRS for a continuum emission of a point source $S^{PSC}(\lambda)$ in Jy.

5. HIGH RESOLUTION SPECTROMETER (HRS)

5.1 Spectral Format

HRS has a short slit with a size of 4" length and 1.7" width. The incoming light through the long slit is cross dispersed via the Echelle grating and cross disperser so that the spectrum over 34 different orders from 85^{th} to 118^{th}, which successively covers the wavelengths from 12.14μm to 17.03μm, and those over 8 different orders from 77^{th} to 84^{th}, which partly covers the wavelengths from 17.03μm to 18.75μm, falls on the 1K×1K Si:As BIB detector array. The plate scale is 0.67 arcsec pix^{-1}.

5.2 Noise Equivalent Electron per Pixel per Exposure

The 1-σ noise equivalent electrons per pixel per second at a certain pixel position X in the m^{th} order spectrum of SMI/HRS, $\phi_m^{NE}(X)$ e^- sec^{-1}, satisfies the following equation

$\phi_m^{NE}(X)\ t_{exp} = \{\phi_m^{NE}(X)\ t_{exp} + \phi_m^{BG}(X)\ t_{exp} + i_{Si:As}^{dark}\ t_{exp} + (n_{Si:As}^{read})^2\}^{1/2}$,

where $\phi_m^{BG}(X)$ is a number of electrons generated at X in the m^{th} order spectrum of HRS by uniform background. Taking account of the available information of the point spread function, pixel-to-wavelength relations for the m^{th} order spectrum (i.e., $\lambda=\Lambda_m(X)$) and the efficiency of the Echelle grating and cross disperser based on the latest design of optics, the values of $\phi_m^{NE}(X)\ t_{exp}$, $\{\phi_m^{BG}(X)\ t_{exp}\}^{1/2}$, $(i_{Si:As}^{dark}\ t_{exp})^{1/2}$ and $n_{Si:As}^{read}$ are calculated and shown in Figure 16 as a function of $\lambda\ (=\Lambda_m(X))$.

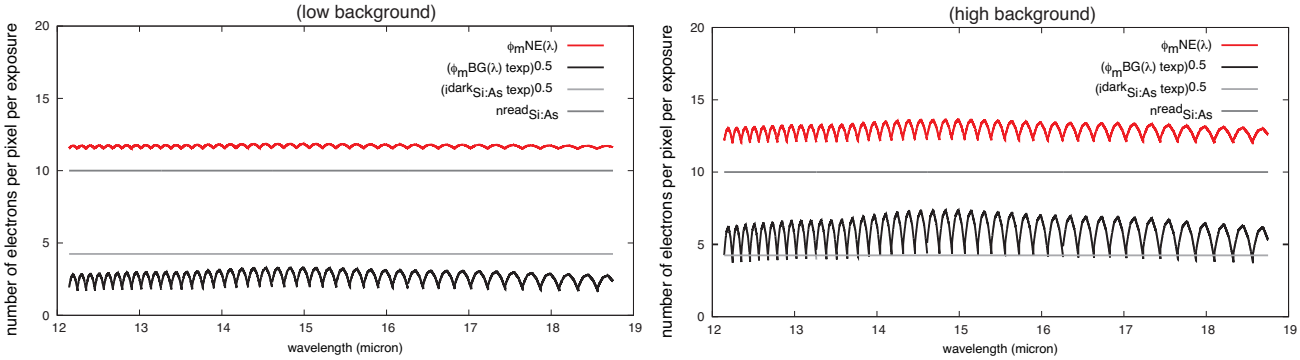

Figure 16. The plots of $\phi_m^{NE}(X)\ t_{exp}$, $\{\phi_m^{BG}(X)\ t_{exp}\}^{1/2}$, $(i_{Si:As}^{dark}\ t_{exp})^{1/2}$ and $n_{Si:As}^{read}$ as a function of $\lambda\ (=\Lambda_m(X))$..

5.3 Sensitivity Estimate for the SMI/HRS

The 1-hour 5-σ sensitivities of SMI/HRS for a continuum emission of a point source ($s^{PSC}(\lambda)$ in units of mJy) calculated for the adopted spectral resolution of R=λ/Δλ. the 1-hour 5-σ sensitivities of SMI/HRS for a line emission of a point source ($s^{PSL}(\lambda)$ in units of Wm^{-2}), the 1-hour 5-σ sensitivities of SMI/HRS for a continuum emission of an extended source ($s^{ESC}(\lambda)$ in units of MJy/sr) calculated for the adopted spectral resolution of R=λ/Δλ and the 1-hour 5-σ sensitivities of SMI/HRS for a line emission of an extended source ($s^{ESL}(\lambda)$ in units of $Wm^{-2}sr^{-1}$) are shown in Figures 17, 18, 19 and 20, respectively. The calculations are made independently for both the low- and high-background cases.

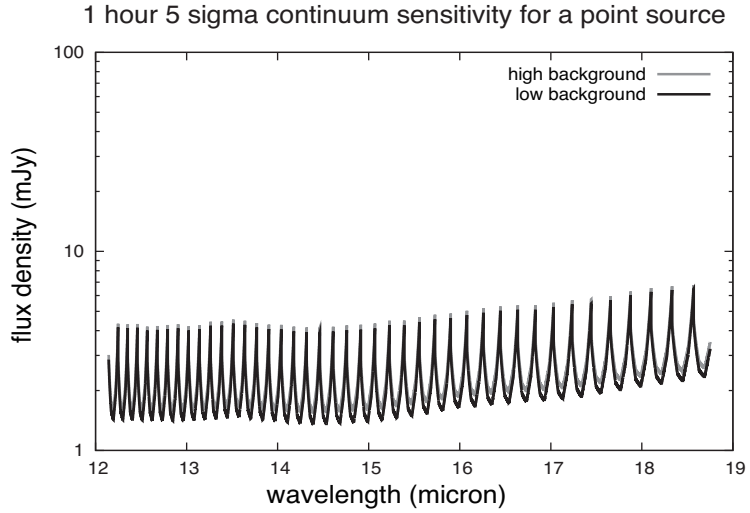

Figure 17. 1-hour 5-σ sensitivities of SMI/HRS for a continuum emission of a point source $s^{PSC}(\lambda)$ in mJy calculated for the adopted spectral resolution of R=λ/Δλ.

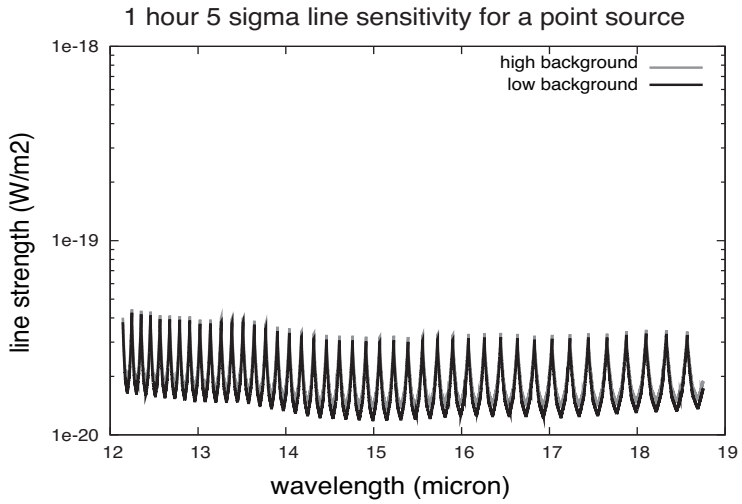

Figure 18. 1-hour 5-σ sensitivities of SMI/HRS for a line emission of a point source $s^{PSL}(\lambda)$ in Wm^{-2}.

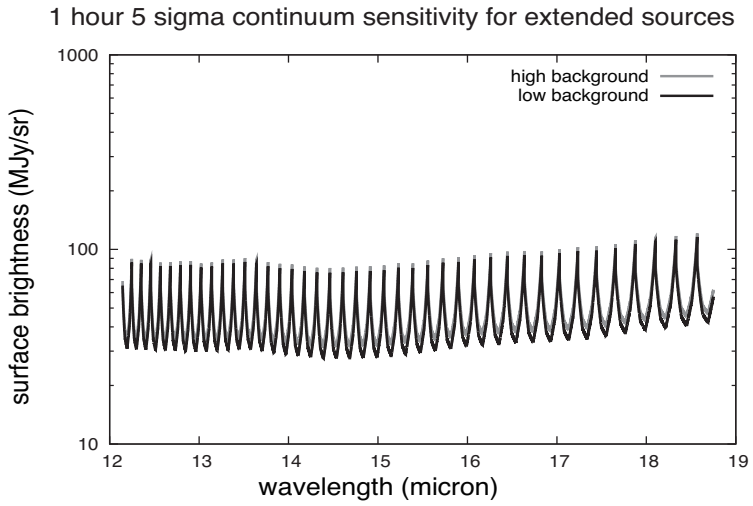

Figure 19. 1-hour 5-σ sensitivities of SMI/HRS for a continuum emission of an extended source $s^{ESC}(\lambda)$ in MJy/sr calculated for the adopted spectral resolution of $R=\lambda/\Delta\lambda$.

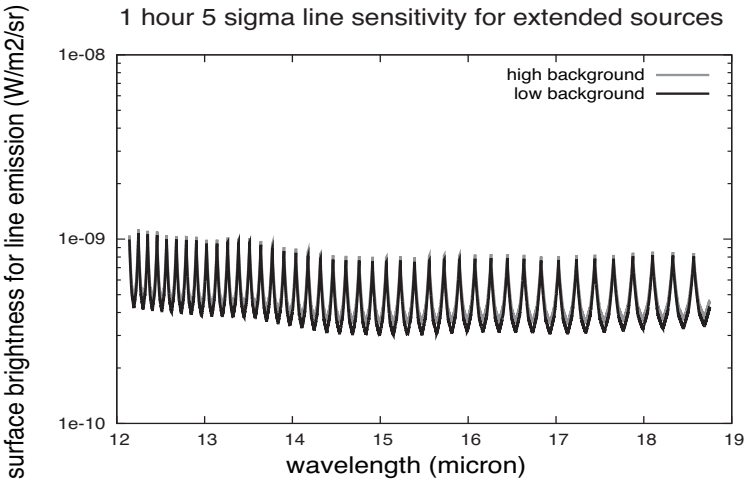

Figure 20. 1-hour 5-σ sensitivities of SMI/HRS for a line emission of an extended source $s^{ESL}(\lambda)$ in $Wm^{-2}\ sr^{-1}$.

5.4 Saturation limit of SMI/HRS

The saturation limits of SMI/HRS for a continuum emission of a point source ($S^{PSC}(\lambda)$ in units of Jy) are shown in Figure 21. The calculations are made independently for both the low- and high-background cases. We note that the data points for both cases are indistinguishable at the scale of this plot.

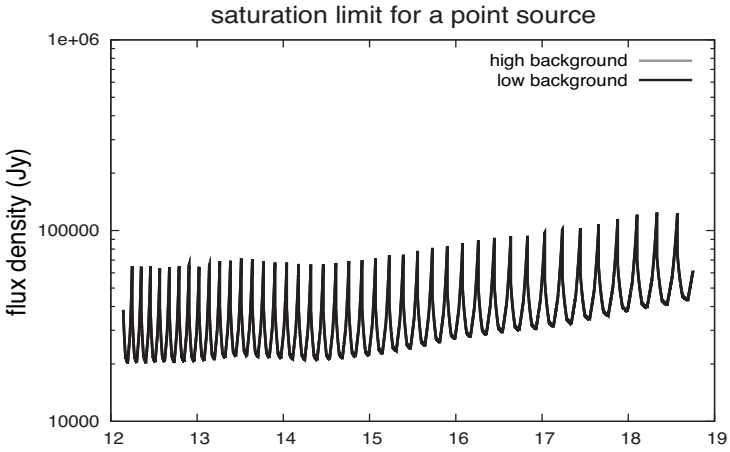

Figure 21. The saturation limit of SMI/HRS for a continuum emission of a point source $S^{PSC}(\lambda)$ in Jy.

ACKNOWLEDGEMENT

This work is supported in part by a Grant-in-Aid for Young Scientists (A) (Grant Number 16H05997)

REFERENCES

[1] Kaneda, H., Ishihara, D., Oyabu, S., Yamagishi, M., Wada, T., Kawada, M., Isobe, N., Asano, K., Suzuki, T., Sakon, I., Tsumura, K., Shibai, H., Matsuo, T., "SPICA mid-infrared instrument (SMI): technical concepts and scientific capabilities", Proc. SPIE, 9904, in this volume (2016)

[2] Swinyard, B. M., Rieke, G. H., Ressler, M., Glasse, A., Wright, G. S., Gerlet, M., Wells, M., "Sensitivity estimates for the mid-infrared instrument (MIRI) on the JWST", Proc. SPIE, 5487, 785-793 (2004)

[3] Reach, W. T., Morris, P., Boulanger, F., Okumura, K., "The mid-infrared spectrum of the zodiacal and exozodiacal light", Icarus, 164, 384-403 (2003)

[4] Ootsubo, T., Onaka, T., Yamamura, I., Tanabe, T., Roellig, T. L., Chan, K.-W., Matsumoto, T., "IRTS Observations of the Mid-Infrared Spectrum of the Zodiacal Emission", Advances in Space Research, 25, 2163-2166 (2000)